Astronomy & Astrophysics manuscript no. arxiv
February 5, 2014
©ESO 2014

Dark Matter Massive Fermions and Einasto Profiles in Galactic Haloes

I. Siutsou, C. R. Argüelles, and R. Ruffini

International Center of Relativistic Astrophysics Network (ICRANet), Piazza della Repubblica 10, 65122 Pescara, Italy.
Dipartimento di Fisica, Università degli Studi di Roma "Sapienza", P.le Aldo Moro 5, 00185 Roma, Italy.

Received / Accepted

ABSTRACT

On the basis of a fermionic dark matter model we fit rotation curves of The HI Nearby Galaxy Survey THINGS sample and compare our 3-parametric model to other models widely used in the literature: 2-parametric Navarro–Frenk–White, pseudoisothermal sphere, Burkhert models, and 3-parametric Einasto model, suggested as the new "standard dark matter profile" model in the paper by Chemin et. al., AJ 142 (2011) 109. The results from the fitting procedure provides evidence for an underlying fermionic nature of the dark matter candidate, with rest mass above the keV regime.

Key words. Dark matter – Astroparticle physics – Galaxies: halos – Galaxies: kinematics and dynamics

arXiv:1402.0695v1 [astro-ph.GA] 4 Feb 2014

1. Introduction

The problem of the distribution of Dark Matter (DM) in galaxies, as usually addressed in the literature, is mainly focused in the halo regions and associated with the galaxy rotation curves obtained from the observations, see e.g. Einasto (2013). A well-known approach used to deal with this problem is the Navarro–Frenk–White (NFW) model (Navarro et al. 1997), expected to provide a universal description of dark matter halos obtained under the following main considerations: 1) N-body simulations in Cold dark matter (CDM) and (ΛCDM) cosmologies; 2) particles each of masses of $\sim 10^9 M_\odot$ [1]; 3) classical Newtonian physics.

Despite an indicated agreement of this model with the large scale structure of the Universe, some problems remains at galactic scales, see e.g. Munshi et al. (2013). A central characteristic of the NFW dark matter density profiles, is that they show a cuspy and divergent behaviour through the center of the configuration, while empirical profiles tend to show a core of constant density, giving rise to the well-known core-cusp controversy, see e.g. de Blok (2010).

Yet another important approach developed to understand the distribution of matter in galaxies has been advanced by Einasto (1965) and Einasto & Haud (1989). This is a phenomenological approach consisting in the proposal of an empirical fitting function composed by three free parameters as detailed in equation (1)

$$\rho_E(r) = \rho_{-2} \exp\left(-\frac{2}{n}\left[\left(\frac{r}{r_{-2}}\right)^n - 1\right]\right), \quad (1)$$

where ρ_{-2} and r_{-2} are the density and radius at which $\rho(r) \propto r^{-2}$, and n is the Einasto index which determines the shape of the profile.

Recent N-body simulations in ΛCDM cosmology by Navarro et al. (2004) purported a novel dark matter halo model different from NFW. This model was soon realized (Merritt et al. 2006) to be the same as the Einasto one as given by equation (1).

After that, using the highest quality rotation curves available to date obtained from The HI Nearby Galaxy Survey (THINGS) (Walter et al. 2008; de Blok et al. 2008), the Einasto dark matter halo model has been proposed as the standard model for dark matter halos by Chemin et al. (2011), as it provides both cored and cusped distributions for different values of model parameters (see Fig. 1). In that work, the fundamental core-cusp discrepancy is analyzed in detail for the whole sample of galaxies under study. It is clearly shown that for the majority of the galaxies considered in the sample, the cored halos (compatible with near unity Einasto indexes) are preferred over the cuspy ones (these instead compatible with higher Einasto indexes).

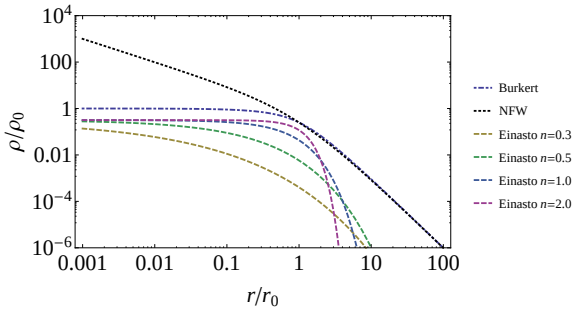

Fig. 1. Comparison of the density profiles for different phenomenological models of dark matter distribution.

We present here a novel approach focusing on galactic structures and an underlying microphysical component of Dark Matter. The model is built upon the following general considerations: 1) the Dark Matter component is assumed to be chargeless spin-1/2 fermions; 2) the configurations are described by General Relativity; 3) the particles are assumed to be isothermal in thermodynamic equilibrium (i.e. without the need of pre-

Send offprint requests to: I. Siutsou, e-mail: siutsou@icranet.org
[1] Modern numerical simulations can reach better resolution down to particle masses of $\sim 10^5 M_\odot$ (Gao et al. 2012).

fixing any cosmological history). The theoretical fundament of this new approach is detailed in the model of semi-degenerate self-gravitating fermions first introduced by Gao et al. (1990), and more recently with applications to galactic dark matter by Ruffini et al. (2013); Argüelles et al. (2013). Our model is based in the following main assumptions:

1. the problem of galactic cores and halos have to be addressed unitarily;
2. for definiteness we study the simplest problem of "bare" massive particles, neglecting at this stage all other interactions than the gravitational one and fulfilling only the Fermi–Dirac statistical distribution

$$f = \frac{1}{\exp\left(\frac{\epsilon-\mu}{kT}\right)+1} = \frac{1}{\exp\left(\frac{\epsilon}{\beta mc^2}-\theta\right)+1}, \tag{2}$$

where ϵ is kinetic energy of the particles, μ is chemical potential, T is the temperature, k is Boltzmann constant and c is the speed of light. The mass of the particle (m), the temperature parameter ($\beta = kT/mc^2$) and the degeneracy parameter ($\theta = \mu/kT$) at the center are the three free parameters of the model;
3. we consider zero total angular momentum and also neglect any effect of baryonic matter on the DM in the mathematical formulation.

It is shown that in any such system the density at large radii scales as r^{-2} independently of the values of the central density, providing the flat rotation curve (Gao et al. 1990; Ruffini et al. 2013; Argüelles et al. 2013).

The dark matter halos obtained in the new dark matter approach proposed here share a common or universal feature which shed more light on the core-cusp discrepancy, while providing a new mass scale to the dark matter candidate. Our density profiles always favor a cored behaviour (without any cusp) in the observed inner halo regions, given the quantum nature of the fermionic particles. Another fundamental outcome of our model is the range of the DM particle mass, which must be $m \gtrsim 5$ keV in order to be in agreement with typical halo sizes of the observed dwarf galaxies (Ruffini et al. 2013).

The theoretical formulation of Ruffini et al. (2013); Argüelles et al. (2013) is based on the first principles physics and provides a physical complement to Einasto phenomenological models. It also offers the necessity to approach the Dark Matter distribution in galactic haloes with fermions with masses larger than the above mentioned bound.

The paper is structured as follows. We model the distribution of Dark Matter as semidegenerate fully relaxed thermal self-gravitating general relativistic fermionic solutions of Gao et al. (1990), see Sec. 2. The resulting density profiles provide flat rotation curve at large distances, cored distribution of dark matter in the halo, and a massive degenerate core at the very center, see Sec. 3. We describe in Sec. 4 the actual procedure of fitting of rotation curves, and then discuss the results in Sec. 5. Conclusions follow.

2. Model equations

We consider self-gravitating system of fermions in thermal equilibrium following Gao et al. (1990) with occupation numbers given by

$$f(\epsilon) = \frac{1}{e^{\frac{\epsilon-\mu}{kT}}+1}. \tag{3}$$

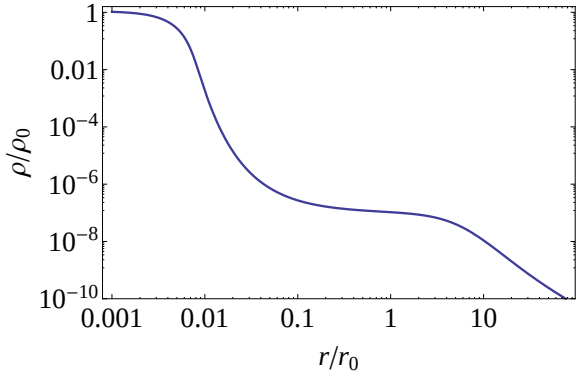

Fig. 2. Semidegenerate density profile in dimensionless units for central degeneracy parameter $\theta_0 = 15$ and central temperature parameter $\beta_0 = 10^{-10}$.

Then equation of state reads

$$\rho = m\frac{g}{h^3}\int \frac{1+\epsilon/mc^2}{e^{\frac{\epsilon-\mu}{kT}}+1}\,d^3p, \tag{4}$$

$$P = \frac{2}{3}\frac{g}{h^3}\int \frac{(1+\epsilon/mc^2)^{-1}(1+\epsilon/2mc^2)\epsilon}{e^{\frac{\epsilon-\mu}{kT}}+1}\,d^3p, \tag{5}$$

where $g = 2s+1$, s is the spin of the particle, and integration is extended over all 3-momentum space.

The Einstein equations for the spherically symmetric metric

$$g_{\mu\nu} = \mathrm{diag}(e^{\nu}, -e^{\lambda}, -r^2, -r^2\sin^2\theta), \tag{6}$$

where ν and λ depend only on the radial coordinate r, together with the thermodynamic equilibrium conditions of Tolman (1930) and Klein (1949)

$$e^{\nu/2}T = const\,, \qquad e^{\nu/2}(\mu+mc^2) = const, \tag{7}$$

can be written in the dimensionless form of Gao et al. (1990)

$$\frac{d\hat{M}}{d\hat{r}} = 4\pi\hat{r}^2\hat{\rho}, \tag{8}$$

$$\frac{d\theta}{d\hat{r}} = -\frac{1-\beta_0(\theta-\theta_0)}{\beta_0}\,\frac{\hat{M}+4\pi\hat{P}\hat{r}^3}{\hat{r}^2(1-2\hat{M}/\hat{r})}, \tag{9}$$

$$\frac{d\nu}{d\hat{r}} = \frac{\hat{M}+4\pi\hat{P}\hat{r}^3}{\hat{r}^2(1-2\hat{M}/\hat{r})}, \tag{10}$$

$$\beta_0 = \beta(r)e^{\frac{\nu(r)-\nu_0}{2}}, \tag{11}$$

$$e^{-\lambda} = 1-\frac{2\hat{M}(\hat{r})}{\hat{r}}\,. \tag{12}$$

The following dimensionless quantities were introduced:

$$\hat{r} = r/\chi, \tag{13}$$

$$\hat{M} = GM/(c^2\chi), \tag{14}$$

$$\hat{\rho} = G\chi^2\rho/c^2, \tag{15}$$

$$\hat{P} = G\chi^2P/c^4, \tag{16}$$

where $\chi = 2\pi^{3/2}(\hbar/mc)(m_p/m)$ is the characteristic length that scales as m^{-2}, with $m_p = \sqrt{\hbar c/G}$ being the Planck mass, and the temperature and degeneracy parameters, $\beta = kT/(mc^2)$ and $\theta = \mu/(kT)$, respectively. The constants of the equilibrium conditions

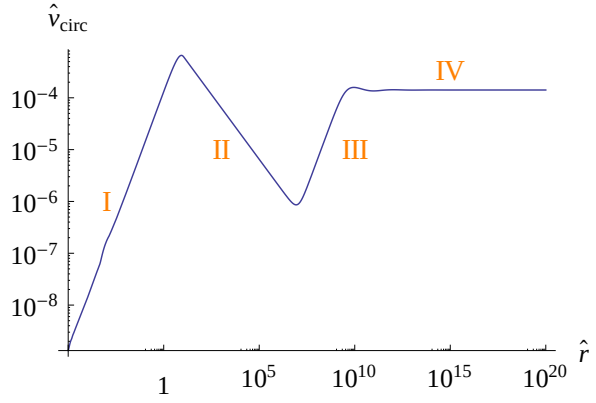

Fig. 3. Dependence of $\hat{v}_{\rm circ} = v_{\rm circ}/c$ on dimensionless radius $\hat{r}$, $\beta = 10^{-8}$, $\theta_0 = 50$.

of Tolman and Klein have been evaluated at the center $r = 0$, which we indicate with a subscript '0'.

The system of coupled differential equations (8–12) is solved for initial conditions $M(0) = \nu(0) = 0$ and given set of free parameters β_0 and θ_0, m for each galaxy under study as detailed below.

3. Properties of semidegenerate configurations

Galactic halos have to be necessarily composed from cold particles, so that astrophysically relevant solutions will have temperature parameters $\beta \ll 1$. In this case, the general solution for semidegenerate configurations ($\theta_0 \gtrsim 10$) present three different regions: an inner degenerate compact core, an extended low-degenerate inner halo of almost constant density and a non-degenerate outer halo with characteristic slope $\rho \propto r^{-2}$ (see Gao et al. (1990) and Fig. 2 for additional details). The infinite mass of the configuration extended up to spatial infinity is not a problem, because in reality it is limited by tidal interactions with other galaxies, which introduce an energy cutoff into the distribution function, see e.g. Ingrosso et al. (1992). However this is not important for the inner parts of the configuration we are interested in.

In order to understand the crucial properties of this equilibrium configurations we plot the circular velocity of a test body in the metric fulfilling Eqs. (8–12) on Fig. 3. There are indeed four regions of the solution for circular velocity, each with characteristic slope. The inner region I correspond to the degenerate core of almost constant density, so that $v_{\rm circ} \propto r$. For increasing values of radial coordinate the inner halo follows, itself composed of two different regions. In the region II the density of dark matter sharply decreases and this Keplerian region is dominated by the mass of the degenerate core, and as a result $v_{\rm circ} \propto r^{-1/2}$. For yet increasing values of the radial coordinate the density of dark matter reach an almost constant value giving rise to a plateau, see Fig. 2. As soon as the mass of the plateau prevails over the mass of the core we have the region III where $v_{\rm circ} \propto r$. Finally in the region IV, after some oscillations the circular velocity tends to a constant independent on r, corresponding to a pure Boltzmannian regime and characteristic for the flat rotation curve of outer halo.

We define the physical characteristics of each configuration as follows:

- The characteristic radius of the core $\hat{r}_c$ is given by $\hat{v}_{\rm circ}(\hat{r}_c) =$ max in region I.
- $\hat{M}_c$ is the mass of the core given by $\hat{M}_c = \hat{v}^2_{\rm circ}\hat{r}$ in the region II.
- The characteristic radius of the inner halo $\hat{r}_h$ correspond to $\hat{v}_{\rm circ}(\hat{r}_h) =$ max in region III.
- The characteristic mass of the inner halo $\hat{M}_h$ is given by $\hat{M}_h = \hat{M}(\hat{r}_h)$ just between the regions III and IV.

For the parameters in the region of $\theta_0 \in [0, 200], \log\beta_0 \in [-10, -5]$ we calculate a grid of models and extracted numerically the physical characteristics mentioned above. Then we fit the obtained values by different double parametric functions and find out the best fitting formulae with the correspondent (β_0,θ_0) dependence for the range of $\theta_0 \in [20, 200]$. An interesting fact is that in our region of parameters circular velocity $v_{\rm circ}$ in the flat part of region IV (i.e. v_∞) is defined by temperature β_0 only. In the range of astrophysically relevant parameters $\theta_0 \in [10, 200], \log\beta_0 \in [-10, -5]$ the scaling relation between circular velocity and β_0 corresponds to the Boltzmannian relation between $v_{\rm circ}$ and one-dimensional dispersion velocity $\sigma = \sqrt{kT/m}$ (see e.g. Binney & Tremaine (1987))

$$\frac{v_\infty}{\rm km/s} = \sqrt{2}c\sqrt{\beta_0}. \tag{17}$$

We have here neglected general relativistic corrections which are very small in these ranges of parameters, i.e. $e^{\nu(\infty)-\nu(0)} \approx 1$, and then $\beta(\infty) \approx \beta_0$ by equation (11).

For the temperature and degeneracy free parameters in the range $\log\beta_0 \in [-10, -5]$, $\theta_0 \in [20, 200]$, respectively, we obtain the following dimensionless scaling laws for core radius and mass[2]

$$\hat{r}_c = 0.226(\beta_0\theta_0)^{-1/4}, \tag{18}$$

$$\hat{M}_c = 0.234(\beta_0\theta_0)^{3/4}. \tag{19}$$

However, the core region is typically very small and is not constrained by empirical data of the THINGS sample considered here. Moreover, the mass contribution of regions I and II to the total mass M_h at the end of region III is $\lesssim 10^{-2}$ in our parameter range as shown in Ruffini et al. (2013), indicating that only regions III and IV are the relevant ones to be used in the fitting procedure against the data.

At this point it is important to emphasize that the theoretical treatment used here to fit dark matter halos applies for any core size, even for the ones which are close to its critical mass, $M_{cr} \sim 10^9 M_\odot$, as studied in Argüelles et al. (2014), where a relativistic treatment is mandatory. Even though the regions I-II-III-IV corresponding to the sample considered here can be well explained in terms of non-relativistic physics, the general relativistic approach has been used for formal correctness, only giving negligible corrections.

Dimensionless halo radius and mass have different scalings, they are proportional not to θ_0^α, but to α^{θ_0}

$$\hat{r}_h = 0.953\beta_0^{1/4}(1.445)^{\theta_0}, \tag{20}$$

$$\hat{M}_h = 2.454\beta_0^{3/4}(1.445)^{\theta_0}. \tag{21}$$

[2] For radii $r < r_c$ the configurations corresponds to region I, where $\rho(r) \approx const$ and then from (18) and (19), taking into account (13) and (14), we can write $\rho_c \propto M_c/r_c^3$ in terms of the chemical potential and particle mass ($\beta_0\theta_0 = \mu_0/mc^2$) as $\rho_c \propto \mu_0^{3/2}m^{5/2}$. This dependence is precisely the one of a fully degenerate non-relativistic Fermi gas in presence of an external gravitational field, which is further coinciding with a polytrope of index $n = 3/2$ (see e.g. Shapiro & Teukolsky (1983)).

Formulas (20–21) represent perfect scalings in the region of parameters considered above, which involves also the scaling of the whole rotational curves in regions III and IV; formula (17) shows a perfect scaling in the flat part of the rotation curve for region IV. Moreover, the Newtonian expression for the dimensionless circular velocity $\hat{v}^2_{circ}(\hat{r}) = \hat{M}/\hat{r}$ is perfectly suitable in the physical region under consideration. The expression for maximal rotation velocity in the halo is thus obtained from (20) and (21) and reads

$$\hat{v}^2_h(\hat{r}_h(\beta_0, \theta_0)) = 2.575\beta_0^{1/2}. \quad (22)$$

In next section we explain the fitting procedure with the use of the halo scaling laws for regions III and IV obtained here.

4. Observed rotation curves and fitting procedure

In 2008, a sample of 34 nearby (closer than 15 Mpc) spiral and irregular galaxies (Sb to Im) were observed with The HI Nearby Galaxy Survey (THINGS) (Walter et al. 2008). These observations allowed to obtain the highest quality rotation curves available to date due to the high spatial and velocity resolution of THINGS. Then a sub-sample of these rotation curves, corresponding to 19 rotationally dominated and undisturbed galaxies, were combined with information on the distribution of gas and stars by de Blok et al. (2008) to construct mass models for the dark matter component of the sample. These models finally were used to quantify the dark matter contribution for each galaxy by using the following formula

$$V^2_{obs} = V^2_{gas} + \Upsilon_* V^2_* + V^2_{DM}, \quad (23)$$

which relates the observed input curves of V_{obs}, V_{gas} and V_*, defined below, with the dark matter rotation curve V_{DM} to be determined from the known input data once the the mass-to-light ratio Υ_* is provided.

The total and gas observed rotation curves V_{obs} and V_{gas}, respectively, were both obtained from the THINGS data: the first was obtained from velocity fields analysis and the second from the neutral hydrogen (HI) distribution maps, as described in de Blok et al. (2008). Instead, each stellar (light) rotation curve V_* is obtained from the corresponding stellar distribution observed in the K band (i.e. at 3.6 μm) by the *Spitzer* Infrared Nearby Galaxy Survey (SINGS), independent of THINGS, and described in de Blok et al. (2008) and references therein. Finally, the mass-to-light ratio Υ^K_* was used to determine the rotation curve associated with the stellar mass distribution from that of the measured light.

At this point it is relevant to further emphasize the underlying hypothesis to which equation (23) is subject to. This is, each baryonic rotation velocity V_{gas} and V_* was calculated from the correspondent observed baryonic mass density distribution, and was defined as the velocity that each component would induce on a test particle in the galactic plane as if they were isolated of any external influence.

In de Blok et al. (2008) equation (23) was applied to test the cuspy Navarro-Frenk-White and cored pseudo-ISO dark matter models against data as follows: the (squared) rotation curves of the baryonic components (after appropriate scaling with Υ^K_*) were subtracted from the (squared) observed rotation curve V^2_{obs} to apply a reduced χ^2 fitting procedure in order to find the best fitting free parameters for each dark matter model. Soon after, the same analysis was extended further to Einasto dark matter profiles by Chemin et al. (2011), concluding that the Einasto model provides the best match to the observed rotation curves when compared with NFW and pseudo-ISO models with empirical fixed values for Υ^K_* for two different stellar initial mass functions (IMFs).

Here we propose a different dark matter halo model, which is neither based on numerical N-body simulations nor on phenomenological model proposals, but relies on the underlying microphysical composition of the dark matter candidate, as explained in former sections.

Thus, analogously to de Blok et al. (2008) and Chemin et al. (2011) we use the HI high resolution observations of galaxies from THINGS survey (Walter et al. 2008). We analyze here the sample of 16 rotationally dominated and undisturbed galaxies presented both in de Blok et al. (2008) and Chemin et al. (2011), listed below in Table 1.

Regarding the rotation curves data of the baryonic components, we consider the contributions of the gas, the stellar disk and a spherical stellar bulge V_b as given in Chemin et al. (2011). The halo rotation velocity corresponding to the spherical dark matter component is taken from the two parametric scaling, see (20–21), which we name from now on as the fermionic dark matter velocity profile $V_f(r)$.

Once each component is provided, we make use of the equation analogous to (23)

$$V^2_{obs} = V^2_{gas} + \Upsilon_* V^2_* + V^2_b + V^2_f, \quad (24)$$

With all the baryonic velocity terms (V^2_{gas}, $\Upsilon_* V^2_*$ and V^2_b) as observational inputs, we fit the HI observed rotation curve V^2_{obs} by Levenberg–Marquardt nonlinear least-squares algorithm, in complete analogy as done in Chemin et al. (2011).

We did not take into account the contribution of molecular gas because the total gas surface densities are dominated by atomic gas for the majority of the sample, as explained in Chemin et al. (2011) and references therein. Total rotation curve was taken from de Blok et al. (2008). We have not considered models with free mass-to-light ratios, deferring it to a future paper (in preparation). Instead following Chemin et al. (2011) we have adopted the fixed mass-to-light ratios of stellar populations with a bursty star formation history with a Kroupa IMF. We choose this IMF instead of the diet-Salpeter IMF, also considered in Chemin et al. (2011) and de Blok et al. (2008), as it generally provides better agreement with observations for rotation curves (see Fig. 5 of Chemin et al. (2011)), and in some cases the Salpeter IMF leads to rotational velocities due to stellar component only already in pronounced excess over observed total rotational velocity (see, for example, cases of NGC3521 and NGC5055 at Fig. 3 of Chemin et al. (2011)).

Together with the dark matter profile of semidegenerate configurations with particle mass $m = 10$ keV/c^2 and varying θ_0 and β_0, and for the sake of comparison, the following profiles were also used for fitting:

- Cored profiles with central density ρ_0 and characteristic radius r_0:
  - pseudo-isothermal sphere profile

$$\rho_{DM}(r) = \rho_0 \frac{r_0^2}{r^2 + r_0^2}, \quad (25)$$

  - Burkert profile

$$\rho_{DM}(r) = \rho_0 \frac{r_0^3}{(r_0 + r)(r_0^2 + r^2)}. \quad (26)$$

– Cusped profiles with characteristic radius r_{-2} where the density profile has a (logarithmic) slope of -2 (the "isothermal" value) and ρ_{-2} as the local density at that radius. In the case of Einasto profiles a third parameter is needed, the Einasto index n which determines the shape of the profile.
  – Navarro–Frenk–White profile

$$\rho_{DM}(r) = 4\rho_{-2}\frac{r_{-2}}{r}\left(\frac{r_{-2}}{r+r_{-2}}\right)^2, \tag{27}$$

  – Einasto profile[3]

$$\rho_{DM}(r) = \rho_{-2}\exp\left\{-2n\left[\left(\frac{r}{r_{-2}}\right)^{1/n} - 1\right]\right\}. \tag{28}$$

5. Results and discussion

In this section, we compare the fits of rotation curves by the different models considered in the last section. As we have to compare models with different number of parameters, which are not nested into each other, we use Bayesian Information Criterion (BIC) introduced by Schwarz (1978). It provides a penalty to models with larger number of parameters to check what of them is more likely to be correct. Model with minimum BIC value is preferred. For the models with the same number of parameters, BIC is equivalent to χ^2 criterion.

The results of fitting are presented in the Table 1 and on Fig. 4. Due to the scaling laws recalled in Sec. 3 the fits obtained here for particle mass $m = 10$ keV/c^2 can be also transferred to another particle mass by changing the fitted central degeneracy parameter from θ_0^* (see Table 1) according to the relation

$$\theta_0(m) = \theta_0^* + 12.52\log\frac{m}{10\ \mathrm{keV}/c^2}, \tag{29}$$

provided that $\theta_0(m)$ is larger than 20 and the influence of the degenerate core on rotational velocity is negligible in the observed radial range. From the values of θ_0^* obtained for the fitting of the sample listed in Table 1, and the lower value of $\theta_0(m)$ from which the scaling laws (18–21) are valid, it is possible to obtain from (29) a preliminary lower limit for the particle mass $m \gtrsim$ few keV/c^2. Nonetheless this limit should not be considered as an absolute lower limit for the fermion mass of the model because the bound $\theta_0(m) \geqslant 20$ in the formula above is a numerical limit, and no underlying physics has been specified here for it. The formal way of providing an absolute lower limit for the particle mass of our model when applied to typical spiral galaxies has been found in Ruffini et al. (2013), and yields roughly an order of magnitude less than the one inferred here.

From the 16 galaxies analyzed, our model has minimum BIC value in 5 cases (NGC2366, NGC2841, NGC2903, NGC2976, NGC3521), Einasto model in 10 cases (NGC2403, NGC3031, IC2574, NGC3621, NGC4736, DDO154, NGC5055, NGC6946, NGC7331, NGC7793), and in the case of NGC3198 Burkert model is the best one, marginally better than ours, which in turn is marginally better than Einasto. Besides this general comparison in which apparently Einasto model is preferred against our model, there is a more relevant comparison which must be made considering that the semi-degenerate model provides cored halos only. For this, we compare the Einasto model against the semi-degenerate one for the sub-set of galaxies which are cored-like (i.e. with Einasto index $n \lesssim 4$), and then the same comparison is made for the sub-set of galaxies which are cuspy-like (i.e. with Einasto index $n > 4$). The important outcome of this new BIC comparison is that our model is *equivalently* as good as Einasto for the cored-like sub-sample, that is connected to the fact that Einasto profile with $n \sim 1$ provides rotational curves that in a wide range of radii is quite close to the one of ours at transition from region III to region IV. For cored-like galaxies in 6 cases our model has lower BIC number than Einasto model (NGC2366, NGC2841, NGC2903, NGC2976, NGC3198, NGC3521), and inversely in other 6 cases Einasto is better (NGC3031, IC2574, NGC4736, DDO154, NGC5055, NGC7793). Instead, for the cuspy-like sub-sample (NGC2403, NGC3621, NGC6946, NGC7331), in *all* the cases Einasto model has lower BIC numbers as logically one may expect due to the cored nature of the semi-degenerate halos.

If we take only the models with significant fits, i.e. with reduced χ^2 less than one at least for one fit, then our model is preferred in 3 cases (NGC2366, NGC2903, NGC2976), Einasto one in 5 cases (NGC2403, IC2574, NGC3621, DDO154, NGC7331), and Burkert fit for NGC3198 is also significant. It is remarkable that neither Navarro–Frenk–White model, nor pseudo-ISO model is preferred against others in the THINGS sample.

If we take into account only two-parametric models, then we have the same 5 aforementioned cases for our model to be the best plus the case of NGC5055, NFW model is preferred in 2 cases (NGC2403, NGC6946), pseudo-ISO one in 3 cases (NGC3621, DDO154, NGC7331), and Burkert model in 5 cases (NGC3031, NGC3198, IC2574, NGC4736, NGC7331). Taking only significant fits, we get the best performance of our model in 3 cases (NGC2366, NGC2903, NGC2976), NFW in 1 case of NGC2403, pseudo-ISO in 2 cases (DDO154, NGC7331), and Burkert in 2 cases (NGC3198, IC2574). From this we can conclude that our model is the best two-parametric model of the set considered.

It is interesting to make pair comparison of our model with Burkert profile: it is preferred statistically in 6 cases (NGC2366, NGC2841, NGC2903, NGC2976, NGC3521, NGC5055) and is disfavored in 10 cases. However, in all these cases besides IC2574 the preference is only marginal.

It should be mentioned that the velocity profile of the semidegenerate configuration used for fitting is exact only in the case of Dark Matter domination and thermal equilibrium at all radii, that can be not the case of real galaxies. However, it is especially interesting that even such a simplified model provides good correspondence to empirical rotational curves.

6. Conclusion

It follows from the results of fitting that the semidegenerate fermionic distributions can fit dark matter in the THINGS sample of galaxies at least as well as other profiles considered in the literature, with the important "revenue" that this profile is theoretically motivated, and is not phenomenological as most of the others. The cases when Einasto profile fits rotational curve much better than semidegenerate profile show the general cuspy behaviour of dark matter distribution, possibly representing a special class of galaxies that are still not completely relaxed.

While Einasto profile is a pure phenomenological one based on best fit of the observational and numerical simulation data, our profile is derived from the first principles and based on the General Relativistic treatment of self-gravitating neutral

[3] The family of Einasto profiles with relatively large indices $n > 4$ are identified with cuspy halos, while low index values $n < 4$ presents a cored-like behaviour (Chemin et al. 2011). The lower the n the more cored-like the halo profile.

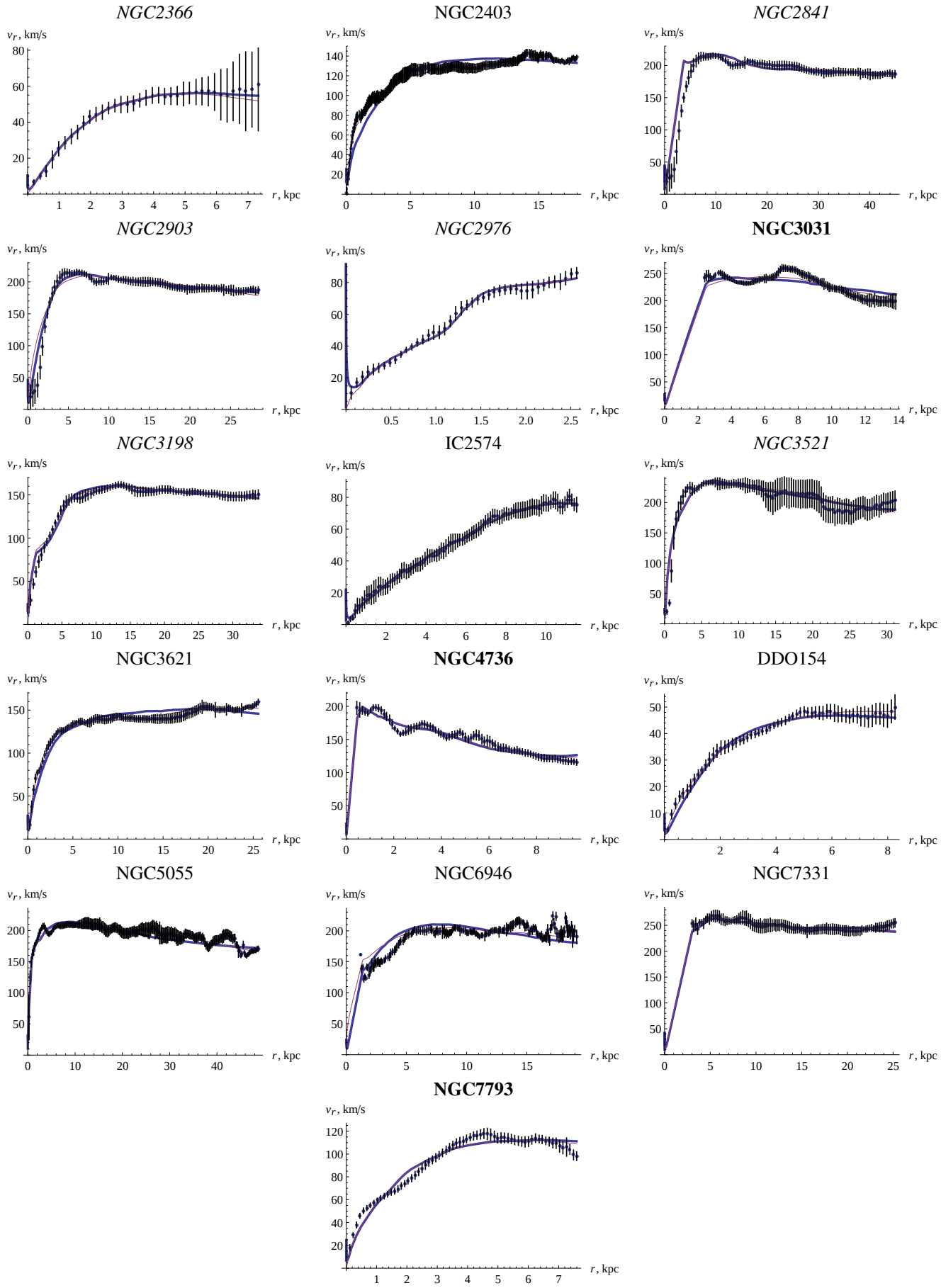

Fig. 4. Rotational curves $v_r(r)$ for some galaxies from THINGS survey together with fits. Blue thick curves show best fits by dark matter distributions of semidegenerate configurations, while magenta thin curves show Einasto profile best fits. Galaxy names where semidegenerate profile fits rotation curves better than Einasto profile are emphasized, and names where profiles are comparable in fit quality are bolded. See digital version for colored plots.

Table 1. Results of fitting

	Semidegenerate				Burkert			
Galaxy	$\beta, 10^{-8}$	θ_0^*	χ_r^2	BIC	r_0, kpc	ρ_0, 10^{-3} $M_\odot/\mathrm{pc}^3$	χ_r^2	BIC
NGC2366	0.99 ± 0.02	24.22 ± 0.08	0.10	*27*	2.2 ± 0.2	43 ± 10	0.12	35
NGC2403	7.10 ± 0.06	27.43 ± 0.07	2.7	902	4.08 ± 0.06	83 ± 3	2.3	866
NGC2841	10.8 ± 0.4	32.04 ± 0.17	2.6	*366*	20.6 ± 0.9	5.2 ± 0.5	2.7	370
NGC2903	16.33 ± 0.09	26.88 ± 0.06	0.66	*238*	2.89 ± 0.06	388 ± 18	1.1	283
NGC2976	9 ± 3	28.8 ± 0.4	0.44	*93*	20 ± 20	40 ± 150	0.49	97
NGC3031	9.7 ± 0.3	26.6 ± 0.2	3.9	470	2.63 ± 0.10	270 ± 20	3.9	468
NGC3198	7.44 ± 0.07	28.66 ± 0.08	1.06	254	6.32 ± 0.18	36 ± 2	0.99	*248*
IC2574	2.00 ± 0.06	27.96 ± 0.09	0.28	167	8.0 ± 0.6	7.2 ± 1.2	0.10	67
NGC3521	8.9 ± 0.7	28.3 ± 0.4	4.1	*437*	5.4 ± 0.4	60 ± 8	4.2	437
NGC3621	7.35 ± 0.11	28.70 ± 0.08	3.0	496	6.48 ± 0.12	34.3 ± 1.3	2.5	475
NGC4736	3.01 ± 0.13	22.4 ± 0.5	2.1	302	0.84 ± 0.07	870 ± 160	1.9	296
DDO154	0.791 ± 0.017	24.37 ± 0.10	0.84	172	2.32 ± 0.10	29 ± 3	0.62	153
NGC5055	8.35 ± 0.13	30.99 ± 0.12	1.9	708	14.3 ± 0.5	8.0 ± 0.5	2.0	719
NGC6946	8.9 ± 0.3	26.9 ± 0.2	16.4	993	3.48 ± 0.08	146 ± 7	15.7	985
NGC7331	11.7 ± 0.2	30.10 ± 0.12	0.45	226	9.7 ± 0.7	25 ± 4	0.41	214
NGC7793	4.44 ± 0.16	25.85 ± 0.13	3.7	287	2.60 ± 0.07	130 ± 8	3.5	284

	Navarro–Frenk–White				Pseudo-ISO			
Galaxy	r_{-2}, kpc	ρ_{-2}, 10^{-3} $M_\odot/\mathrm{pc}^3$	χ_r^2	BIC	r_0, kpc	ρ_0, 10^{-3} $M_\odot/\mathrm{pc}^3$	χ_r^2	BIC
NGC2366	200 ± 1100	0.02 ± 0.24	1.1	117	1.29 ± 0.17	40 ± 11	0.15	42
NGC2403	11.2 ± 0.3	2.86 ± 0.17	0.7	575	1.56 ± 0.04	144 ± 8	1.2	703
NGC2841	150 ± 30	0.05 ± 0.02	3.8	402	12.5 ± 0.7	4.6 ± 0.6	2.8	374
NGC2903	4.75 ± 0.16	34 ± 2	1.8	334	0.53 ± 0.05	2300 ± 500	3.9	406
NGC2976	900 ± 40000	0.009 ± 1	2.1	158	9 ± 18	30 ± 180	0.49	98
NGC3031	4.9 ± 0.4	20 ± 3	4.0	472	0.82 ± 0.1	690 ± 170	4.3	480
NGC3198	16.5 ± 0.9	1.37 ± 0.15	2.0	306	2.7 ± 0.14	51 ± 5	1.2	266
IC2574	500 ± 1300	0.007 ± 0.045	1.5	331	5.1 ± 0.4	6.3 ± 1.1	0.11	70
NGC3521	18 ± 3	1.5 ± 0.4	5.1	457	2.4 ± 0.3	78 ± 19	4.2	439
NGC3621	123 ± 17	0.08 ± 0.02	5.9	579	2.81 ± 0.09	49 ± 3	1.1	377
NGC4736	1.25 ± 0.16	90 ± 20	1.9	296	0 ± 0.07	0 ± ND	2.3	311
DDO154	14 ± 2	0.35 ± 0.11	1.03	184	1.22 ± 0.07	32 ± 4	0.48	138
NGC5055	48 ± 4	0.20 ± 0.03	3.0	795	7.8 ± 0.4	7.7 ± 0.8	2.5	759
NGC6946	9.3 ± 0.4	5.3 ± 0.5	10.4	915	0.66 ± 0.03	870 ± 70	11.0	923
NGC7331	3000 ± 40000	0.004 ± 0.087	0.48	233	5. ± 0.5	28 ± 6	0.32	190
NGC7793	17.0 ± 1.9	1.4 ± 0.3	4.1	294	1.47 ± 0.05	126 ± 10	4.0	293

	Einasto				
Galaxy	r_{-2}, kpc	ρ_{-2}, 10^{-3} $M_\odot/\mathrm{pc}^3$	n	χ_r^2	BIC
NGC2366	2.9 ± 0.4	6.86 ± 0.04	0.9 ± 0.3	0.13	39
NGC2403	13.6 ± 1.3	1.98 ± 0.05	4.9 ± 0.4	0.6	*570*
NGC2841	24.5 ± 0.6	1.091 ± 0.006	0.54 ± 0.08	2.5	367
NGC2903	5.33 ± 0.15	28.983 ± 0.005	2.9 ± 0.2	1.6	326
NGC2976	70000 ± ND	0.019 ± ND	4.0 ± 70	0.49	100
NGC3031	4.81 ± 0.09	30.159 ± 0.002	0.56 ± 0.07	3.2	*452*
NGC3198	11.5 ± 0.4	3.029 ± 0.006	1.80 ± 0.17	1.1	257
IC2574	8.6 ± 1.2	1.57 ± 0.05	0.7 ± 0.2	0.09	*62*
NGC3521	9.3 ± 0.5	6.27 ± 0.02	1.2 ± 0.3	4.3	443
NGC3621	37 ± 10	0.3 ± 0.4	6.1 ± 0.9	0.57	*296*
NGC4736	1.73 ± 0.16	56.78 ± 0.03	2.0 ± 0.5	1.8	*295*
DDO154	4.9 ± 0.7	1.95 ± 0.03	2.0 ± 0.3	0.31	*114*
NGC5055	21.4 ± 0.4	1.464 ± 0.002	0.39 ± 0.04	1.2	*626*
NGC6946	50 ± 40	0.2 ± 4	15 ± 4	8.5	*883*
NGC7331	1000 ± 8000	0.002 ± 900	11 ± 21	0.23	*158*
NGC7793	3.65 ± 0.14	19.217 ± 0.007	0.97 ± 0.09	3.1	*279*

ND means not constrained model parameters

fermions. There is the distinct possibility that our treatment gives the conceptual physical motivation for the existence of the cored Einasto profile directly from the structure of the microphysical constituents of dark matter.

Acknowledgements. The authors wish to thank Prof. Herman Mosquera Cuesta for critical reading of the manuscript and valuable suggestions.

References

Argüelles, C. R., Fraga, B., & Ruffini, R. 2014, Journal of the Korean Physical Society (submitted)
Argüelles, C. R., Ruffini, R., Siutsou, I., & Fraga, B. 2013, Journal of the Korean Physical Society (submitted)
Binney, J. & Tremaine, S. 1987, Galactic dynamics (Princeton University Press)
Chemin, L., de Blok, W. J. G., & Mamon, G. A. 2011, AJ, 142, 109
de Blok, W. J. G. 2010, Advances in Astronomy, 2010
de Blok, W. J. G., Walter, F., Brinks, E., et al. 2008, AJ, 136, 2648
Einasto, J. 1965, Trudy Astrofizicheskogo Instituta Alma-Ata, 5, 87
Einasto, J. 2013, Brazilian Journal of Physics, 43, 369
Einasto, J. & Haud, U. 1989, A&A, 223, 89
Gao, J. G., Merafina, M., & Ruffini, R. 1990, A&A, 235, 1
Gao, L., Navarro, J. F., Frenk, C. S., et al. 2012, MNRAS, 425, 2169
Ingrosso, G., Merafina, M., Ruffini, R., & Strafella, F. 1992, A&A, 258, 223
Klein, O. 1949, Reviews of Modern Physics, 21, 531
Merritt, D., Graham, A. W., Moore, B., Diemand, J., & Terzić, B. 2006, AJ, 132, 2685
Munshi, F., Governato, F., Brooks, A. M., et al. 2013, ApJ, 766, 56
Navarro, J. F., Frenk, C. S., & White, S. D. M. 1997, ApJ, 490, 493
Navarro, J. F., Hayashi, E., Power, C., et al. 2004, MNRAS, 349, 1039
Ruffini, R., Argüelles, C. R., Rueda, J. A., & Siutsou, I. 2013, Phys. Rev. Lett.(to be submitted)
Schwarz, G. E. 1978, Annals of Statistics, 6, 461

Shapiro, S. L. & Teukolsky, S. A. 1983, Black holes, white dwarfs, and neutron stars: The physics of compact objects (Wiley-Interscience)
Tolman, R. C. 1930, Physical Review, 35, 904
Walter, F., Brinks, E., de Blok, W. J. G., et al. 2008, AJ, 136, 2563